JOURNAL OF COMPUTATIONAL PHYSICS **131,** 199–215 (1997)
ARTICLE NO. CP965602

An Upwind Difference Scheme for the Double-Adiabatic Equations

Rudolf Wegmann

Max-Planck-Institut für Astrophysik, Karl-Schwarzschildstrasse 1, 85748 Garching, Germany

Received December 4, 1995; revised September 10, 1996

An upstream differencing numerical scheme is devised for the double-adiabatic equations which describe a plasma with anisotropic pressure. The Godunov-type method uses an approximate Riemann solver, which is constructed with an explicit representation of the complete eigensystem of the Jacobian matrix of the flux vector. A correction term is introduced into the numerical flux which allows switching off the instabilities. One- and three-dimensional test calculations show that the method works well for stable and unstable flows. For the latter the instabilities tend to isotropize the pressure so that the flow becomes stable. First results of calculations for the interaction of the solar wind with a comet show that the pressure anisotropies due to the ion pickup modify the plasma flow considerably.

1. INTRODUCTION

The nucleus of a comet consists of a mixture of ice and dust. Irradiated by the sun the ice sublimates. Gases streaming away from the nucleus form a cloud of neutral molecules which by various processes are ionized with a time scale of about 10^6 s. The solar wind is a parallel flow of magnetized plasma consisting mainly of protons and electrons. The cometary ions are implanted into the solar wind as soon as they are generated. By this pickup of slow and heavy ions the solar wind is decelerated and heated. A shock transforms the kinetic energy into thermal energy which then is used to accelerate the ions into the tail. This interaction has since long been successfully described by the equations of ideal magnetohydrodynamics (MHD) with source terms (Schmidt and Wegmann [21, 22]).

The pickup ions at first gyrate around the magnetic field and so form in velocity space a ring distribution, which only gradually is transformed by pitch angle scattering into a shell distribution. This picture has been confirmed by measurements of the Giotto spacecraft near comet Halley [16].

Therefore, the ion pickup has the effect, that the ion pressure becomes anisotropic. A plasma with anisotropic pressure can be described by the double-adiabatic equations derived by Chew, Goldberger, and Low [4] (CGL equations, for short). The most serious approximation in these equations is the neglect of the heat transport parallel to the magnetic field.

Up to now there have been only few numerical calculations using the CGL equations (see [11] for an example). Apparently there has been no theoretical work on numerical methods for these equations.

The treatment of the MHD equations by an upwind difference scheme has first been described and applied on an unstructured grid by Schmidt and Wegmann [21]. This approach becomes now more and more appreciated [3, 24, 23, 25, 6, 7, 10, 20]. The scheme of Munz [15] has also been extended to MHD. The method is based on an approximate Riemann solver. It can also handle discontinuities such as shocks. It can be modified by various methods to make it second order accurate in regions where the flow is smooth (see LeVeque [13] for a survey).

The upwind difference scheme is particularly attractive when the complete eigensystem of the Jacobian matrix of the flux vector can be calculated explicitly. It has been shown by Schmidt and Wegmann [21] that then the upstream correction can be calculated in a very simple way.

The plan of this paper is as follows: We present the double-adiabatic equations. In Section 3 we calculate the Jacobi matrix of the flux function. From this we get an explicit representation of the complete eigensystem. For comparison we give also the derivation for the ideal MHD equations. The upstream differencing numerical scheme is described in Section 5.

For the CGL equations the eigenvalues may become complex. These complex eigenvalues correspond to physical instabilities, namely the mirror and firehose instabilities. In case one might choose to suppress the instabilities in the CGL equations to obtain equilibrium solutions, a method for doing so is described in Section 4. The result of the calculation may then be interpreted as a background state on which the instabilities evolve. For the purpose of illustration we report in Section 6 the results of some test calculations as well as the first results of model calculations for the interaction of the solar wind with a comet.

2. THE DOUBLE-ADIABATIC EQUATIONS

The plasma is described by the following variables: mass density ρ, number density n, an isotropic electron pressure p_e with adiabatic index γ, the two components $p_\perp$ and $p_\parallel$

0021-9991/97 $25.00

of the ion pressure, the bulk velocity $\mathbf{u}$, and the magnetic field $\mathbf{B}$. These quantities are connected by the equations

$$\frac{\partial n}{\partial t} + \operatorname{div}(n\mathbf{u}) = \dot{n} \tag{2.1}$$

$$\frac{\partial \rho}{\partial t} + \operatorname{div}(\rho\mathbf{u}) = \dot{\rho}, \tag{2.2}$$

$$\frac{\partial p_e}{\partial t} + \operatorname{div}(p_e\mathbf{u}) + (\gamma - 1)p_e \operatorname{div}\mathbf{u} = \dot{p}_e, \tag{2.3}$$

$$\frac{\partial p_\perp}{\partial t} + \operatorname{div}(p_\perp\mathbf{u}) + p_\perp \operatorname{div}_\perp\mathbf{u} = \dot{p}_\perp, \tag{2.4}$$

$$\frac{\partial p_\parallel}{\partial t} + \operatorname{div}(p_\parallel\mathbf{u}) + 2p_\parallel \operatorname{div}_\parallel\mathbf{u} = \dot{p}_\parallel, \tag{2.5}$$

$$\frac{\partial \rho\mathbf{u}}{\partial t} + \operatorname{div}(\rho\mathbf{u}\mathbf{u}') + \operatorname{div}\mathbf{P} + \frac{1}{\mu}\operatorname{grad}\frac{B^2}{2} - \frac{1}{\mu}\operatorname{div}(\mathbf{B}\mathbf{B}') + \left(\frac{1}{\mu} - \frac{p_\parallel - p_\perp}{B^2}\right)\mathbf{B}\operatorname{div}\mathbf{B} = \dot{\mathbf{q}}, \tag{2.6}$$

$$\frac{\partial \mathbf{B}}{\partial t} + \operatorname{div}(\mathbf{B}\mathbf{u}') - \operatorname{div}(\mathbf{u}\mathbf{B}') + \mathbf{u}\operatorname{div}\mathbf{B} = 0. \tag{2.7}$$

Vectors $\mathbf{v}$ and matrices $\mathbf{M}$ are denoted by boldface letters. A prime indicates the transpose of a vector. In the general case of a complex matrix $\mathbf{M}$ the conjugate transpose is $\mathbf{M}'$. By grad $\mathbf{u}$ we mean the matrix (grad u_x, grad u_y, grad u_z). Let $\mathbf{b} := \mathbf{B}/B$ be a unit vector in the direction of the field. Then $\operatorname{div}_\parallel\mathbf{u} := \mathbf{b}'(\operatorname{grad}\mathbf{u})\mathbf{b}$ is the part of the divergence of the flow field parallel to the magnetic field and $\operatorname{div}_\perp\mathbf{u} := \operatorname{div}\mathbf{u} - \operatorname{div}_\parallel\mathbf{u}$ is the perpendicular part.

The pressure tensor

$$\mathbf{P} = (p_e + p_\perp)\mathbf{I} + (p_\parallel - p_\perp)\mathbf{b}\mathbf{b}' \tag{2.8}$$

is anisotropic. $\mathbf{I}$ denotes the 3×3 identity matrix. The divergence of a matrix is formed rowwise, i.e.,

$$\operatorname{div}\begin{pmatrix}\mathbf{r}_x'\\ \mathbf{r}_y'\\ \mathbf{r}_z'\end{pmatrix} := \begin{pmatrix}\operatorname{div}\mathbf{r}_x\\ \operatorname{div}\mathbf{r}_y\\ \operatorname{div}\mathbf{r}_z\end{pmatrix}.$$

Equations (2.4) and (2.5) are quite analogous to (2.3). The perpendicular and parallel pressures react to a compression perpendicular and parallel to the magnetic field like the pressure of an ideal gas with adiabatic index 2 or 3, respectively, corresponding to the two degrees of freedom across the field and one degree of freedom along the field. The thermal energy is $E_{th} = p_\perp + \frac{1}{2}p_\parallel$. It corresponds to an isotropic pressure $p_{iso} = \frac{2}{3}p_\perp + \frac{1}{3}p_\parallel$ with an effective $\gamma = \frac{5}{3}$.

The right-hand sides in Equations (2.1) to (2.6) describe the addition of new cometary ions into the plasma. These quantities will be specified later. We use separate equations for particles and mass density so that the fraction of cometary ions in the plasma can be determined.

The induction equation (2.7) ensures that the condition $\operatorname{div}\mathbf{B} = 0$ is satisfied for all times if it is satisfied initially. There are several reasons to include the terms proportional to div $\mathbf{B}$ into the equations. Formally the term in (2.7) comes from the flux conservation condition (see [17]). The term in (2.6) removes the term proportional to div $\mathbf{B}$ which comes from the formal transformation of the Lorentz force $(1/\mu)\mathbf{B} \times \operatorname{curl}\mathbf{B}$ and the anisotropic pressure force.

It has been noted by Brackbill and Barnes [2] that the MHD equations without the div $\mathbf{B}$-terms may yield unphysical results when, as a consequence of numerical errors, the condition $\operatorname{div}\mathbf{B} = 0$ is violated. We will see in the next section how div $\mathbf{B}$ can influence the flow if it is not properly included into the equations.

From the induction equation (2.7) follows the conservation law for ''magnetic monopoles''

$$\frac{\partial(\operatorname{div}\mathbf{B})}{\partial t} + \operatorname{div}(\mathbf{u}\operatorname{div}\mathbf{B}) = 0. \tag{2.9}$$

This means that the artificial monopoles are passively convected and finally swept out from the domain of calculations [21, 10]. From the conventional form $\partial\mathbf{B}/\partial t - \operatorname{curl}(\mathbf{u} \times \mathbf{B}) = 0$ follows $\partial(\operatorname{div}\mathbf{B})/\partial t = 0$. This means that monopoles stay where they are generated and errors in div $\mathbf{B}$ can accumulate.

The conservation of the total energy

$$E = \frac{\rho u^2}{2} + \frac{p_e}{\gamma - 1} + p_\perp + \frac{p_\parallel}{2} + \frac{B^2}{2\mu} \tag{2.10}$$

is described by the equation

$$\frac{\partial E}{\partial t} + \operatorname{div}\left(\frac{\rho u^2}{2} + \frac{\gamma p_e}{\gamma - 1} + 2p_\perp + \frac{p_\parallel}{2} + \frac{B^2}{\mu}\right)\mathbf{u} + \operatorname{div}\left((\mathbf{u},\mathbf{B})\left(\frac{p_\parallel - p_\perp}{B^2} - \frac{1}{\mu}\right)\mathbf{B}\right) - \left(\frac{p_\parallel - p_\perp}{B^2} - \frac{1}{\mu}\right)(\mathbf{u},\mathbf{B})\operatorname{div}\mathbf{B} = \dot{E}. \tag{2.11}$$

For ideal MHD the pressure $p = p_\parallel = p_\perp$ is isotropic. It satisfies the same equation

$$\frac{\partial p}{\partial t} + \operatorname{div}(p\mathbf{u}) + (\gamma - 1)p\operatorname{div}\mathbf{u} = \dot{p}, \tag{2.12}$$

as the electron pressure. The momentum equation (2.6) simplifies to

$$\frac{\partial \rho \mathbf{u}}{\partial t} + \operatorname{div}(\rho \mathbf{u}\mathbf{u}') + \operatorname{grad}\left(p_e + p + \frac{B^2}{2\mu}\right) - \frac{1}{\mu}\operatorname{div}(\mathbf{B}\mathbf{B}') + \frac{1}{\mu}\mathbf{B}\operatorname{div}\mathbf{B} = \dot{\mathbf{q}}. \tag{2.13}$$

3. EIGENANALYSIS

We can write the system of equations in a more compact form by combining all physical variables to a vector $\mathbf{V}$ with 11 components:

$$\mathbf{V}' := (n, \rho, p_e, p_\perp, p_\parallel, \mathbf{u}', \mathbf{B}'). \tag{3.1}$$

With the time derivative $d/dt := \partial/\partial t + (\mathbf{u}, \operatorname{grad})$ the equations assume the form

$$\frac{d\mathbf{V}}{dt} + \mathbf{A}_x \frac{\partial \mathbf{V}}{\partial x} + A_y \frac{\partial \mathbf{V}}{\partial y} + \mathbf{A}_z \frac{\partial \mathbf{V}}{\partial z} = \dot{\mathbf{V}} \tag{3.2}$$

with 11×11 matrices $\mathbf{A}_x$, $\mathbf{A}_y$, $\mathbf{A}_z$ which depend on the flow variables $\mathbf{V}$ and on the direction of differentiation which in (3.2) is along one of the unit vectors $\mathbf{e}_x$, $\mathbf{e}_y$, and $\mathbf{e}_z$ in the orthogonal coordinate system x, y, z.

We can quite generally calculate the matrix $\mathbf{A}$ which occurs for differentiation along a unit vector $\mathbf{k}$. One has to put $\mathbf{k} = \mathbf{e}_x, \mathbf{e}_y$, or $\mathbf{e}_z$ in (3.3)–(3.7) to get the matrices $\mathbf{A}_x$, $\mathbf{A}_y$, and $\mathbf{A}_z$ of Eq. (3.2). The matrix $\mathbf{A}$ has block structure

$$\mathbf{A} = \begin{pmatrix} 0 & \mathbf{A}_{12} & 0 \\ \mathbf{A}_{21} & 0 & \mathbf{A}_{23} \\ 0 & \mathbf{A}_{32} & 0 \end{pmatrix} \tag{3.3}$$

with a 5×3 matrix $\mathbf{A}_{12}$, a 3×5 matrix $\mathbf{A}_{21}$, and 3×3 matrices $\mathbf{A}_{23}$ and $\mathbf{A}_{32}$. The 0 denotes matrices of appropriate order with zero elements only. The blocks can explicitly be represented in terms of the unit vectors $\mathbf{k}$ and $\mathbf{b}$ in the following way. We use the abbreviations $b_n := (\mathbf{b}, \mathbf{k})$ and $B_n := (\mathbf{B}, \mathbf{k})$:

$$\mathbf{A}_{12} = \begin{pmatrix} n \\ \rho \\ \gamma p_e \\ 2p_\perp \\ p_\parallel \end{pmatrix} \mathbf{k}' + b_n \begin{pmatrix} 0 \\ 0 \\ 0 \\ -p_\perp \\ 2p_\parallel \end{pmatrix} \mathbf{b}', \tag{3.4}$$

$$\mathbf{A}_{21} = \frac{1}{\rho}(\mathbf{k}(0,0,1,1,0) + b_n \mathbf{b}(0,0,0,-1,1)), \tag{3.5}$$

$$\mathbf{A}_{23} = \frac{1}{\rho}\left(\frac{(p_\parallel - p_\perp)b_n}{B}(\mathbf{I} - 2\mathbf{b}\mathbf{b}') + \frac{1}{\mu}\mathbf{k}\mathbf{B}' - \frac{1}{\mu}B_n\mathbf{I}\right), \tag{3.6}$$

$$\mathbf{A}_{32} = \mathbf{B}\mathbf{k}' - B_n\mathbf{I}. \tag{3.7}$$

Let λ be an eigenvalue of $\mathbf{A}$ with left and right eigenvectors $\mathbf{z}$ and $\mathbf{s}$. It is convenient to decompose these vectors into parts $\mathbf{z}_1$ and $\mathbf{s}_1$ of dimension 5 and $\mathbf{s}_2$, $\mathbf{s}_3$, $\mathbf{z}_2$, and $\mathbf{z}_3$ of dimension 3, adapted to the block structure (3.3) of the matrix $\mathbf{A}$. Then the eigenvalue equation $\mathbf{A}\mathbf{s} = \lambda\mathbf{s}$ is equivalent to the following system of equations:

$$\mathbf{A}_{12}\mathbf{s}_2 = \lambda\mathbf{s}_1, \quad \mathbf{A}_{21}\mathbf{s}_1 + \mathbf{A}_{23}\mathbf{s}_3 = \lambda\mathbf{s}_2, \quad \mathbf{A}_{32}\mathbf{s}_2 = \lambda\mathbf{s}_3. \tag{3.8}$$

Similarly, for the left eigenvector $\mathbf{z}'\mathbf{A} = \lambda\mathbf{z}'$ is equivalent to

$$\mathbf{z}_2'\mathbf{A}_{21} = \lambda\mathbf{z}_1', \quad \mathbf{z}_1'\mathbf{A}_{12} + \mathbf{z}_3'\mathbf{A}_{32} = \lambda\mathbf{z}_2', \quad \mathbf{z}_2'\mathbf{A}_{23} = \lambda\mathbf{z}_3'. \tag{3.9}$$

For $\lambda \neq 0$ one can use the first and the third equations from (3.8) to eliminate $\mathbf{s}_1$, and $\mathbf{s}_3$. An eigenvalue problem of dimension 3 remains

$$\mathbf{M}\mathbf{s}_2 = \lambda^2\mathbf{s}_2 \tag{3.10}$$

with the matrix

$$\mathbf{M} = \mathbf{A}_{21}\mathbf{A}_{12} + \mathbf{A}_{23}\mathbf{A}_{32} = b_n^2(a^2 + c_\perp^2 - c_\parallel^2)\mathbf{I} + (a^2 + c_e^2 + 2c_\perp^2)\mathbf{k}\mathbf{k}' - b_n(a^2 + c_\perp^2)(\mathbf{k}\mathbf{b}' + \mathbf{b}\mathbf{k}') + b_n^2(4c_\parallel^2 - c_\perp^2)\mathbf{b}\mathbf{b}' \tag{3.11}$$

with the abbreviations

$$a^2 = \frac{B^2}{\mu\rho}, \quad c_e^2 = \frac{\gamma p_e}{\rho}, \quad c_\perp^2 = \frac{p_\perp}{\rho}, \quad c_\parallel^2 = \frac{p_\parallel}{\rho}. \tag{3.12}$$

Similarly, one can use the first and the third equations from (3.9) to eliminate $\mathbf{z}_1$, and $\mathbf{z}_3$. This leads to the equation

$$\mathbf{z}_2'\mathbf{M} = \lambda^2\mathbf{z}_2'. \tag{3.13}$$

It follows from (3.11) that $\mathbf{M}$ is a multiple of the identity matrix plus a matrix of rank 2 spanned by the vectors $\mathbf{b}$ and $\mathbf{k}$. The matrix $\mathbf{M}$ is symmetric. Therefore, the eigenvalues λ^2 of $\mathbf{M}$ are real. Left and right eigenvectors of $\mathbf{M}$ coincide; i.e., one can choose $\mathbf{z}_2 = \mathbf{s}_2$.

Since the eigenvalues are independent of the coordinate system we can use a representation of the matrix $\mathbf{M}$ in a convenient basis. To this aim we rotate the coordinate

system so that $\mathbf{b}' = (0, 1, 0)$ and $\mathbf{k}' = (\sin\theta, \cos\theta, 0)$. Then $b_n = \cos\theta$ and

$$\mathbf{M} = \begin{pmatrix} a_{11} & a_{12} & 0 \\ a_{21} & a_{22} & 0 \\ 0 & 0 & a_{33} \end{pmatrix} \tag{3.14}$$

with the elements

$$\begin{aligned} a_{11} &= a^2 + c_e^2 \sin^2\theta + c_\perp^2(1 + \sin^2\theta) - c_\parallel^2 \cos^2\theta, \\ a_{12} &= a_{21} = (c_e^2 + c_\perp^2) \sin\theta\cos\theta, \\ a_{22} &= (3c_\parallel^2 + c_e^2) \cos^2\theta, \\ a_{33} &= (a + c_\perp^2 - c_\parallel^2) \cos^2\theta. \end{aligned} \tag{3.15}$$

This matrix has the eigenvalues

$$\begin{aligned} \lambda_{1,2}^2 = \tfrac{1}{2}(a^2 + c_e^2 + c_\perp^2(1 + \sin^2\theta) + 2c_\parallel^2 \cos^2\theta \\ \pm ((a^2 + c_\perp^2(1 + \sin^2\theta) - 4c_\parallel^2 \cos^2\theta \\ + c_e^2(\sin^2\theta - \cos^2\theta))^2 \\ + 4(c_\perp^2 + c_e^2)^2 \sin^2\theta\cos^2\theta)^{1/2}), \end{aligned} \tag{3.16}$$

$$\lambda_3^2 = (a^2 + c_\perp^2 - c_\parallel^2)\cos^2\theta. \tag{3.17}$$

To be specific, λ_1^2 is defined by (3.16) with the positive sign and λ_2^2 with the negative sign. These eigenvalues agree with the previously calculated propagation speeds [14].

The eigenvectors of the matrix $\mathbf{M}$ can be calculated in the following way:

In the general case when $\cos\theta \sin\theta \neq 0$ the vectors $\mathbf{b}$ and $\mathbf{k}$ are neither parallel nor perpendicular. If $a_{12} \neq 0$ then $\lambda_1^2 \neq \lambda_2^2$ and for $\lambda^2 = \lambda_1^2$ and $\lambda^2 = \lambda_2^2$ an eigenvector of $\mathbf{M}$ in the representation (3.14) is given by $\mathbf{s}_2' = (-a_{12}, a_{11} - \lambda^2, 0)$. One can write $\mathbf{s}_2$ in terms of the given vectors $\mathbf{s}_2 = c_1\mathbf{k} + c_2\mathbf{b}$ with $c_1 = -a_{12}/\sin\theta$, $c_2 = a_{11} - \lambda^2 + a_{12}\cot\theta$. If $a_{12} = 0$ the eigenvectors for λ_1^2 and λ_2^2 are simply $(1, 0, 0)' = \mathbf{k}/\sin\theta - \cot\theta\mathbf{b}$ and $(0, 1, 0)' = \mathbf{b}$. An eigenvector for λ_3^2 is $\mathbf{s}_2 = \mathbf{k} \times \mathbf{b}$ which is nonzero since $\mathbf{k}$ and $\mathbf{b}$ are not parallel.

If $\cos\theta \sin\theta = 0$ then the matrix $\mathbf{M}$ is diagonal.

In the special case $\cos\theta = 0$ the vectors $\mathbf{k}$ and $\mathbf{b}$ are orthogonal. Then all elements of $\mathbf{M}$ vanish except $a_{11} = a^2 + c_e^2 + 2c_\perp^2$. This is the eigenvalue λ_1^2 which has eigenvector $\mathbf{k}$.

In the other case $\sin\theta = 0$ the vectors $\mathbf{k}$ and $\mathbf{b}$ are parallel. The matrix elements are $a_{11} = a_{33} = a^2 + c_\perp^2 - c_\parallel^2$ and $a_{22} = 3c_\parallel^2 + c_e^2$. The eigenvalue $\lambda_2^2 = a_{22}$ has eigenvector $\mathbf{b}$. The eigenvectors for the eigenvalues $\lambda_1^2 = \lambda_3^2 = a_{11}$ are perpendicular to $\mathbf{b}$.

For the eigenvalues $\lambda \neq 0$ of $\mathbf{A}$ the complete eigenvectors can be represented by

$$\mathbf{s} = \begin{pmatrix} \frac{1}{\lambda}\mathbf{A}_{12} \\ \mathbf{I} \\ \frac{1}{\lambda}\mathbf{A}_{32} \end{pmatrix} \mathbf{s}_2, \quad \mathbf{z}' = \mathbf{s}_2' \left(\frac{1}{\lambda}\mathbf{A}_{21}, \mathbf{I}, \frac{1}{\lambda}\mathbf{A}_{23} \right) \tag{3.18}$$

in terms of the already determined eigenvector $\mathbf{s}_2$ of $\mathbf{M}$. This is a consequence of (3.8) and (3.9).

If there are l eigenvalues $\lambda^2 \neq 0$ of $\mathbf{M}$, then l is either 1, 2, or 3 as we have seen in the discussion above. The formula (3.18) gives $2l$ linearly independent eigenvectors for the $2l$ nonzero eigenvalues $\pm\lambda$ of $\mathbf{A}$.

For the eigenvalue $\lambda = 0$ we insert the Ansatz $\mathbf{s}' = (\mathbf{s}_1', 0, \mathbf{s}_3')$ into the eigenvalue equation. The system of three equations

$$\mathbf{A}_{21}\mathbf{s}_1 + \mathbf{A}_{23}\mathbf{s}_3 = 0 \tag{3.19}$$

for the eight components of $\mathbf{s}_1$ and $\mathbf{s}_3$ has at least five linearly independent solutions. These yield five linearly independent eigenvectors of the form $\mathbf{s}' = (\mathbf{s}_1', 0, \mathbf{s}_3')$ for the eigenvalue $\lambda = 0$. Therefore, $\lambda = 0$ is an eigenvalue of the matrix $\mathbf{A}$ with geometric multiplicity at least five.

If all eigenvalues of $\mathbf{M}$ are nonzero we get in this way a complete system of 11 left and 11 right eigenvectors of $\mathbf{A}$. Hence the matrix $\mathbf{A}$ is diagonalizable. One can choose the eigenvectors biorthogonal, i.e., $\mathbf{z}_m'\mathbf{s}_j = 0$ for $m \neq j$. Then the spectral representation

$$\mathbf{A} = \sum_{j=1}^{11} \lambda_j \frac{\mathbf{s}_j\mathbf{z}_j'}{\mathbf{z}_j'\mathbf{s}_j} \tag{3.20}$$

is valid. In view of (3.18) the denominator in (3.20) is for eigenvalues $\lambda \neq 0$ equal to

$$\begin{aligned} \mathbf{z}'\mathbf{s} &= \mathbf{s}_2' \left(\frac{1}{\lambda^2}(\mathbf{A}_{21}\mathbf{A}_{12} + \mathbf{A}_{23}\mathbf{A}_{32}) + \mathbf{I} \right)\mathbf{s}_2 \\ &= \mathbf{s}_2' \left(\frac{1}{\lambda^2}\mathbf{M} + \mathbf{I} \right)\mathbf{s}_2 = 2\|\mathbf{s}_2\|^2. \end{aligned} \tag{3.21}$$

Hence the scalar product $\mathbf{z}'\mathbf{s}$ is twice the square of the middle part $\mathbf{s}_2$.

If some eigenvalues of $\mathbf{M}$ are zero a degeneracy can occur as in ideal MHD. Since only the nonzero eigenvalues λ contribute to the spectral representation (3.20) we do not really need the eigenvectors for the eigenvalue $\lambda = 0$.

We recall for comparison the situation for ideal MHD. Here we combine all physical variables to a vector $\mathbf{V}$ with 10 components

$$\mathbf{V}' := (n, \rho, p_e, p, \mathbf{u}'\ \mathbf{B}'). \tag{3.22}$$

In this case the pertaining matrix $\mathbf{A}$ has order 10. It has the same block structure as shown in (3.3). But now $\mathbf{A}_{12}$ is a 4×3 matrix and $\mathbf{A}_{21}$ a 3×4 matrix,

$$\mathbf{A}_{12} = \begin{pmatrix} n \\ \rho \\ \gamma p_e \\ \gamma p \end{pmatrix} \mathbf{k}', \quad \mathbf{A}_{21} = \frac{1}{\rho}\mathbf{k}(0, 0, 1, 1). \tag{3.23}$$

The 3×3 matrices $\mathbf{A}_{23}$ and $\mathbf{A}_{32}$ are

$$\mathbf{A}_{23} = \frac{1}{\mu\rho}(\mathbf{k}\mathbf{B}' - B_n\mathbf{I}), \quad \mathbf{A}_{32} = \mathbf{B}\mathbf{k}' - B_n\mathbf{I}. \tag{3.24}$$

The eigenvectors are split in a similar way as before into parts of dimension 4 and 3. Then the eigenvalue problem reduces to a problem (3.10) with a matrix $\mathbf{M}$ of order 3, which in this case has the form

$$\mathbf{M} = b_n^2 a^2\mathbf{I} + (a^2 + c_e^2 + c^2)\mathbf{k}\mathbf{k}' - a^2 b_n(\mathbf{k}\mathbf{b}' + \mathbf{b}\mathbf{k}') \tag{3.25}$$

with the abbreviations (3.12) and $c^2 := \gamma p/\rho$.

We represent the matrix $\mathbf{M}$ in the same special coordinate system as before, where $\mathbf{b}' = (0, 1, 0)$ and $\mathbf{k}' = (\sin\theta, \cos\theta, 0)$. Using $b_n = \cos\theta$ we get the representation (3.14) with the elements

$$\begin{aligned} a_{11} &= a^2 + (c_e^2 + c^2)\sin^2\theta, \\ a_{12} = a_{21} &= (c_e^2 + c^2)\sin\theta\cos\theta, \\ a_{22} = (c^2 + c_e^2)&\cos^2\theta, \quad a_{33} = a^2\cos^2\theta. \end{aligned} \tag{3.26}$$

This matrix has the eigenvalues

$$\begin{aligned} \lambda_{1,2}^2 = \tfrac{1}{2}&(a^2 + c^2 + c_e^2 \\ &\pm (a^4 + (c^2 + c_e^2)^2 \\ &+ 2a^2(c^2 + c_e^2)(\cos^2\theta - \sin^2\theta))^{1/2}), \end{aligned} \tag{3.27}$$

$$\lambda_3^2 = a^2\cos^2\theta. \tag{3.28}$$

This yields the well-known magnetosonic speeds and the Alfven velocity. One can calculate the eigenvectors in a quite similar way as above for the CGL equations.

Reduced to one spatial dimension, where all quantities depend only on the variables x and t, the flux conservation implies $B_x = \text{const}$. This can be used to eliminate B_x from the system of equations. This is the standard approach to calculate MHD waves and the eigensystem of the Jacobian matrix $\mathbf{A}$ [12]. One-dimensional upwind schemes [3, 24, 6, 19] used this approach. Also multidimensional schemes were based on the eigensystem for the reduced equations in combination with operator splitting [25, 7, 20], although there is no equivalent for the condition $B_x = \text{const}$.

The complete eigensystem for the three-dimensional Jacobian was used 1980 by Schmidt and Wegmann [21] and again by Gombosi *et al.* [10]. These authors emphasized the importance of including div $\mathbf{B}$ in a proper way into the equations in order to minimize the damage done by the numerical monopoles. If the terms containing div $\mathbf{B}$ are omitted from Eq. (2.7) and (2.13) then the Jacobian matrix $\tilde{\mathbf{A}}$ pertaining to this modified system of equations can be written in the form

$$\tilde{\mathbf{A}} = \mathbf{A} - \begin{pmatrix} 0 \\ \mathbf{B} \\ \mathbf{u} \end{pmatrix} (0, 0, \mathbf{k}') \tag{3.29}$$

with the matrix $\mathbf{A}$ as before.

The vector $\tilde{\mathfrak{s}}$ defined by $\tilde{\mathfrak{s}}' := (0, 0, \mathbf{k}')$ is a right and a left eigenvector of $\mathbf{A}$ for the eigenvalue 0. Reduced to one spatial dimension this vector collects the contributions from $\partial B_x/\partial x = \text{div}\ \mathbf{B}$. The properties $\tilde{\mathfrak{s}}'\mathbf{A} = 0$ and $\mathbf{A}\tilde{\mathfrak{s}} = 0$ ensure that as far as possible no div $\mathbf{B}$ is generated and div $\mathbf{B}$ has no effect.

On the other hand, $\tilde{\mathfrak{s}}'\tilde{\mathbf{A}} = -(\mathbf{u}, \mathbf{k})\tilde{\mathfrak{s}}'$ means that div $\mathbf{B}$ is convected back with velocity $(\mathbf{u}, \mathbf{k})$ in a Lagrangian system; i.e., it stays where it is in an Eulerian grid. The equation

$$\tilde{\mathbf{A}}\tilde{\mathfrak{s}} = -\begin{pmatrix} 0 \\ \mathbf{B} \\ \mathbf{u} \end{pmatrix} \tag{3.30}$$

means that div $\mathbf{B}$ really does something; namely it generates velocity, i.e., exerts forces on the flow and generates a new field. Since, in addition, div $\mathbf{B}$ is not convected away by these equations it can become an inexhaustible source of nuisance.

A nonzero div $\mathbf{B}$ is a manifestation of the numerical error. It depends on the situation whether or not this form of numerical error is more dangerous than other manifestations. If need be, div $\mathbf{B}$ can be removed by a projection method [2].

4. INSTABILITIES

The matrix **M** is symmetric. Therefore, the eigenvalues λ^2 are real. Hence the eigenvalues λ are real or imaginary, depending on whether $\lambda^2 \geq 0$ or $\lambda^2 < 0$.

We get immediately from (3.17) that λ_3^2 is negative if and only if $\cos^2\theta > 0$ and

$$c_\parallel^2 - c_\perp^2 > a^2. \tag{4.1}$$

It follows from (3.16) that λ_1^2 is nonnegative. The sign of λ_2^2 depends on the sign of the determinant $D_0 := a_{11}a_{22} - a_{12}^2$. Using (3.15) D_0 can be written in the form $D_0 = D_1 \cos^2\theta$ with

$$\begin{aligned} D_1 &= (c_\perp^2 - c_\parallel^2 + a^2)(3c_\parallel^2 + c_e^2)\cos^2\theta \\ &\quad + (3c_\parallel^2(c_\perp^2 + c_e^2) + (c_\perp^2 + a^2)(3c_\parallel^2 + c_e^2) \\ &\quad - c_\perp^2(c_\perp^2 + c_e^2))\sin^2\theta \\ &= A_1\cos^2\theta + A_2\sin^2\theta. \end{aligned} \tag{4.2}$$

The coefficient A_1 of $\cos^2\theta$ is negative if and only if (4.1) is satisfied. The coefficient A_2 of $\sin^2\theta$ is negative if and only if

$$c_\parallel^2 - c_\perp^2 < -2c_\parallel^2 - \frac{(c_\perp^2 + a^2)(3c_\parallel^2 + c_e^2)}{c_\perp^2 + c_e^2} \tag{4.3}$$

holds, i.e., if the perpendicular pressure exceeds the parallel pressure by a sufficiently large amount.

The conditions (4.1) and (4.3) are mutually exclusive. Therefore, at most one of the coefficients A_1 or A_2 can become negative. Hence $D_1 < 0$ can occur only in a certain θ-interval which is given by

$$\begin{aligned} &\tan^2\theta < -\frac{A_1}{A_2} \quad \text{for } A_1 < 0, \\ &\tan^2\theta > -\frac{A_1}{A_2} \quad \text{for } A_2 < 0. \end{aligned} \tag{4.4}$$

The following three cases can occur:

Case 1. A_1 and A_2 are both nonnegative. Then all $\lambda^2 \geq 0$ for all angles θ.

Case 2. $A_1 < 0$ and $A_2 \geq 0$. Then

$$\begin{aligned} &\lambda_3^2 < 0 \quad \text{for } \tan^2\theta < \infty, \\ &\lambda_2^2 < 0 \quad \text{for } \tan^2\theta < -\frac{A_1}{A_2}. \end{aligned} \tag{4.5}$$

Case 3. $A_1 \geq 0$ and $A_2 < 0$. Then

$$\lambda_2^2 < 0 \quad \text{for } -\frac{A_1}{A_2} < \tan^2\theta < \infty. \tag{4.6}$$

Consider the one-dimensional inhomogeneous linear system of differential equations

$$\frac{\partial \mathbf{U}}{\partial t} + \mathbf{A}\frac{\partial \mathbf{U}}{\partial x} = g(x) \tag{4.7}$$

with a real matrix **A** and the vector **U** of m variables. Assume that **A** has eigenvalues λ_j and a full system of eigenvectors $\mathbf{s}_j$ and $\mathbf{z}_j$ which satisfy the biorthogonality relation $\mathbf{z}_j'\mathbf{s}_k = \delta_{jk}$. Then **A** has the spectral representation

$$\mathbf{A} = \sum \lambda_j \mathbf{s}_j \mathbf{z}_j'. \tag{4.8}$$

If an eigenvalue λ is complex then the corresponding eigenvectors **s** and **z** are also complex. We denote by Re **s** the vector whose components are the real parts of the components of the vector **s**. The vector Im **s** is defined in a similar way. Note that $(\text{Im } \mathbf{z})' = -\text{Im } \mathbf{z}'$, since the prime involves also complex conjugation.

The matrix **A** is real. Therefore, one can replace the right-hand side of (4.8) by its real part. This leads to a decomposition $\mathbf{A} = \mathbf{A}_s + \mathbf{A}_u$ with the matrices

$$\begin{aligned} \mathbf{A}_s &= \sum \text{Re } \lambda_j \text{Re}(\mathbf{s}_j\mathbf{z}_j') \\ &= \sum \text{Re } \lambda_j(\text{Re } \mathbf{s}_j \text{Re } \mathbf{z}_j' + \text{Im } \mathbf{s}_j(\text{Im } \mathbf{z}_j)'), \\ \mathbf{A}_u &= -\sum \text{Im } \lambda_j \text{Im}(\mathbf{s}_j\mathbf{z}_j') \\ &= \sum \text{Im } \lambda_j(\text{Re } \mathbf{s}_j(\text{Im } \mathbf{z}_j)' - \text{Im } \mathbf{s}_j \text{Re } \mathbf{z}_j'). \end{aligned} \tag{4.9}$$

For real eigenvalues λ the eigenvectors can be chosen as real vectors. Complex eigenvalues λ occur in complex conjugate pairs λ, $\bar{\lambda}$. The corresponding eigenvectors can also be chosen as complex conjugate. It follows from the biorthogonality condition that

$$\begin{aligned} \text{Re } \mathbf{z}' \text{Re } \mathbf{s} = (\text{Im } \mathbf{z})' \text{Im } \mathbf{s} = \frac{1}{2}, \\ \text{Re } \mathbf{z}' \text{Im } \mathbf{s} = (\text{Im } \mathbf{z})' \text{Re } \mathbf{s} = 0. \end{aligned} \tag{4.10}$$

This implies that the system $\mathbf{z}_j$ and $\mathbf{s}_j$ remains a biorthogonal system if the conjugate complex pairs **z**, $\bar{\mathbf{z}}$ and **s**, $\bar{\mathbf{s}}$ are replaced by the pairs $\sqrt{2}$Re **z**, $\sqrt{2}$Im **z** and $\sqrt{2}$Re **s**, $\sqrt{2}$Im **s**. It follows that the definition (4.9) of the matrices $\mathbf{A}_s$ and $\mathbf{A}_u$ gives already the spectral representation. Each complex conjugate pair gives twice the same contribution to the sum. This yields the factor 2 which is needed for the normalization of the real and imaginary parts of the

vectors. It turns out that $\mathbf{A}_s$ has only real eigenvalues Re λ_j, while $\mathbf{A}_u$ has besides the trivial eigenvalue $\lambda = 0$, only purely imaginary eigenvalues i Im λ_j. The eigenvectors are the real and imaginary parts of the eigenvectors of the original matrix $\mathbf{A}$.

One can represent the parts of the matrix $\mathbf{A}$ also in the following way:

$$\mathbf{A}_s = \sum \text{Re } \lambda_j \, \mathbf{s}_j \mathbf{z}_j', \quad \mathbf{A}_u = i \sum \text{Im } \lambda_j \, \mathbf{s}_j \mathbf{z}_j'. \tag{4.11}$$

Since complex eigenvalues and eigenvectors occur only in conjugate pairs the imaginary parts of $\mathbf{s}_j \mathbf{z}_j'$ cancel in the first sum of (4.11) while the real parts cancel in the second.

This decomposition of the matrix $\mathbf{A}$ gives rise to a decomposition of the differential equation. If $\mathbf{U}_s$ and $\mathbf{U}_u$ are two vector functions which solve the system of equations

$$\frac{\partial \mathbf{U}_s}{\partial t} + \mathbf{A}_s \frac{\partial \mathbf{U}_s}{\partial x} = g(x), \quad \frac{\partial \mathbf{U}_u}{\partial t} + \mathbf{A} \frac{\partial \mathbf{U}_u}{\partial x} = -\mathbf{A}_u \frac{\partial \mathbf{U}_s}{\partial x} \tag{4.12}$$

then $\mathbf{U} = \mathbf{U}_s + \mathbf{U}_u$ solves Eq. (4.7). The part $\mathbf{U}_s$ is governed by a standard hyperbolic system and remains stable. The second part $\mathbf{U}_u$ describes instabilities which are excited by the right-hand side of the second equation in (4.12).

This simple decomposition into a stable background $\mathbf{U}_s$ and unstable disturbances $\mathbf{U}_u$ seems to be possible only for equations in one space dimension like (4.7). One can formally apply the same decomposition to each of the matrices $\mathbf{A}_x$, $\mathbf{A}_y$, and $\mathbf{A}_z$ in the three-dimensional equation (3.2) but this does, in general, not remove all instabilities.

The CGL equations describe physical instabilities, namely the mirror and the firehose instabilities. Nevertheless the equations may not always be physically meaningful for unstable flows for the following reasons.

First, the shortest waves grow fastest. This leads to an immediate breakdown unless the initial data are very smooth. The initial value problem is no longer well posed. This can be seen most easily by the prototype of an unstable system of equations,

$$\frac{\partial v}{\partial t} + \frac{\partial u}{\partial x} = 0, \quad \frac{\partial u}{\partial t} - \frac{\partial v}{\partial x} = 0 \tag{4.13}$$

for two functions u and v. These are simply the Cauchy–Riemann equations for the real and imaginary parts of an analytic function. Equations (4.13) are elliptic and the initial value problem is not well posed and, therefore, not well suited to describe a physical situation. The pair of equations pertaining to a conjugate complex pair of eigenvalues of the matrix $\mathbf{A}$ can be transformed to the form (4.13) [8].

The nonlinear terms in the CGL equations limit the growth of the instabilities. The pressure becomes more isotropic so that the flow is stabilized.

In reality the plasma is isotropized, not by the macroscopic instabilities as described by the CGL equations, but rather by microinstabilities. Plasma theory predicts the onset of the mirror instability earlier than condition (4.3).

In numerical calculations the fastest growing mode is determined by the grid size and by the numerical method used (see Section 6 for examples). Therefore, one cannot really solve the equations for unstable flow numerically except in cases with very carefully chosen smooth initial conditions.

In view of these objections it may be desirable to suppress the instabilities in the CGL equations and to include, instead, the effect of the microinstabilities in a phenomenological way.

5. DISCRETIZATION

We introduce in addition to the vector $\mathbf{V}$ the vector $\mathbf{W} := (n, \rho, p_e, p_\perp, p_\parallel, \rho\mathbf{u}', \mathbf{B}')$ where the velocity is replaced by the momentum. Equations (2.1)–(2.7) can then be written in compact form,

$$\frac{\partial \mathbf{W}}{\partial t} + \text{div } \mathbf{F} + \mathbf{C}_x(\mathbf{V}) \frac{\partial \mathbf{V}}{\partial x} + \mathbf{C}_y(\mathbf{V}) \frac{\partial \mathbf{V}}{\partial y} + \mathbf{C}_z(\mathbf{V}) \frac{\partial \mathbf{V}}{\partial z} = \dot{\mathbf{W}}. \tag{5.1}$$

The conservative part of the equations is expressed as the divergence of an 11×3 flux matrix

$$\mathbf{F} = \begin{pmatrix} \mathbf{F}_1 \\ \mathbf{F}_2 \\ \mathbf{F}_3 \end{pmatrix} \tag{5.2}$$

which is built up by a 5×3 matrix $\mathbf{F}_1$ and 3×3 matrices $\mathbf{F}_2$ and $\mathbf{F}_3$ of the form

$$\mathbf{F}_1 = \begin{pmatrix} n \\ \rho \\ p_e \\ p_\perp \\ p_\parallel \end{pmatrix} \mathbf{u}', \quad \mathbf{F}_3 = \mathbf{B}\mathbf{u}' - \mathbf{u}\mathbf{B}', \tag{5.3}$$

$$\mathbf{F}_2 = \rho \mathbf{u}\mathbf{u}' + \mathbf{P} + \frac{B^2}{2\mu}\mathbf{I} - \frac{1}{\mu}\mathbf{B}\mathbf{B}'.$$

The columns of $\mathbf{F}$ are the flux vectors $\mathbf{F}^x$, $\mathbf{F}^y$, $\mathbf{F}^z$.

The last terms in (5.1) represent the nonconservative terms. Each of them is written as the product of a matrix

C and a derivative of **V**. The matrix **C** depends on the direction **k** of differentiation. The matrices $\mathbf{C}_x$, $\mathbf{C}_y$, and $\mathbf{C}_z$ are obtained as special cases for $\mathbf{k} = \mathbf{e}_x$, $\mathbf{e}_y$, and $\mathbf{e}_z$ from the following general representation. The block structure of **C** is similar to that of **A**, namely,

$$\mathbf{C} = \begin{pmatrix} 0 & \mathbf{C}_{12} & 0 \\ 0 & 0 & \mathbf{C}_{23} \\ 0 & 0 & \mathbf{C}_{33} \end{pmatrix} \tag{5.4}$$

with the blocks

$$\mathbf{C}_{12} = \begin{pmatrix} 0 \\ 0 \\ (\gamma - 1)p_e \\ p_\perp \\ 0 \end{pmatrix} \mathbf{k}' + b_n \begin{pmatrix} 0 \\ 0 \\ 0 \\ -p_\perp \\ 2p_\parallel \end{pmatrix} \mathbf{b}', \tag{5.5}$$

$$\mathbf{C}_{23} = \left(\frac{1}{\mu} - \frac{p_\parallel - p_\perp}{B^2} \right) \mathbf{B}\mathbf{k}', \quad \mathbf{C}_{33} = \mathbf{u}\mathbf{k}'. \tag{5.6}$$

We consider first a one-dimensional flow where all variables depend only on t and x. Then (5.1) reduces to

$$\frac{\partial \mathbf{W}}{\partial t} + \frac{\partial \mathbf{F}^x(\mathbf{V})}{\partial x} + \mathbf{C}_x(\mathbf{V}) \frac{\partial \mathbf{V}}{\partial x} = \dot{\mathbf{W}}. \tag{5.7}$$

Let Δx be the grid size and Δt the time step. We assume that $\mathbf{V}_j^n$ are the values of **V** at the grid points $x_j = j\Delta x$, $j = 1, ..., N$, at time $t_n = n\Delta t$. It is useful to introduce interfaces at the positions $x_{j+1/2} = (j + \frac{1}{2})\Delta x$, $j = 0, 1, ..., N$. The values at time t_{n+1} are calculated by the formula

$$\mathbf{W}_j^{n+1} = \mathbf{W}_j^n + \Delta t \dot{\mathbf{W}}_j - \frac{\Delta t}{\Delta x} \left(\mathbf{F}^{x,n}_{j+1/2} - \mathbf{F}^{x,n}_{j-1/2} + \mathbf{C}_x(\mathbf{V}_j^n) \frac{\mathbf{V}_{j+1}^n - \mathbf{V}_{j-1}^n}{2} \right). \tag{5.8}$$

Each term on the right side is well defined, except the fluxes $\mathbf{F}^{x,n}_{j\pm1/2}$ at the interfaces.

To calculate these fluxes we proceed as follows. First we define values on the interfaces $\mathbf{V}_{j+1/2} = (\mathbf{V}_j^n + \mathbf{V}_{j+1}^n)/2$ and calculate the Jacobian matrix **A** as described in Section 3 for these values of $\mathbf{V}_{j+1/2}$ with the normal $\mathbf{k} = (1, 0, 0)'$. The eigenvalues and eigenvectors are $\lambda_{j+1/2,l}$, $\mathbf{s}_{j+1/2,l}$, $\mathbf{z}_{j+1/2,l}$, $l = 1, ..., 11$. We assume that these vectors are biorthogonal and normalized.

The matrix **A** occurs in the differential equations (3.2)

$$\frac{d\mathbf{V}}{dt} + \mathbf{A} \frac{\partial \mathbf{V}}{\partial x} = \dot{\mathbf{V}} \tag{5.9}$$

for the vector **V**. The corresponding linearized version of the equations (5.7) for the vector **W** can be written in the form

$$\frac{d\mathbf{W}}{dt} + \mathbf{H}\mathbf{A} \frac{\partial \mathbf{V}}{\partial x} = \dot{\mathbf{W}} \tag{5.10}$$

with the matrix

$$\mathbf{H} = \frac{\partial \mathbf{W}}{\partial \mathbf{V}} = \begin{pmatrix} \mathbf{I} & 0 & 0 \\ \mathbf{H}_{21} & \rho\mathbf{I} & 0 \\ 0 & 0 & \mathbf{I} \end{pmatrix} \tag{5.11}$$

which has the same block structure as **A**. The only nontrivial offdiagonal block is $\mathbf{H}_{21} = \mathbf{u}(0, 1, 0, 0, 0)$.

We have calculated in Section 3 the eigensystem of the matrix **A** which occurs in the formulation (3.2) of the equations in a comoving (Lagrangian) coordinate system. In a fixed (Eulerian) system the derivative $d\mathbf{V}/dt$ in (3.2) is replaced by $\partial\mathbf{V}/\partial t + (\mathbf{u}, \text{grad})\mathbf{V}$. This has the effect that in (3.3) **A** is replaced by $\mathbf{A} + u_n\mathbf{I}$ with $u_n = (\mathbf{u}, \mathbf{k})$ and the identity matrix **I**. The matrices **A** and $\mathbf{A} + u_n\mathbf{I}$ have the same right and left eigenvectors $\mathbf{s}_j$ and $\mathbf{z}_j$. Only the eigenvalues λ_j are Doppler shifted to $\lambda_j + u_n$. This equivalence is used in the following derivation of a difference scheme for Eq. (5.7) in Eulerian coordinates.

For the calculation of the fluxes $\mathbf{F}^n_{j+1/2}$ we proceed as follows. We assume that u_x, **A**, $\mathbf{C}_x$, and **H** are constant in a neighborhood of $x_{j+1/2}$; i.e., $\mathbf{F}^x(\mathbf{V}) = (u_x\mathbf{I} + \mathbf{A} - \mathbf{C}_x)\mathbf{V}$ and $\mathbf{W} = \mathbf{H}\mathbf{V}$. Provisional values $\tilde{\mathbf{V}}$ at $x_{j+1/2}$ are obtained from the condition that for each characteristic variable the value is taken from the adjacent grid cell which is upstream along the pertaining characteristic. This upwinding strategy was recommended by Courant *et al.* [5]. It leads to the system of equations

$$\mathbf{z}'_{j+1/2,l}\tilde{\mathbf{V}} = \begin{cases} \mathbf{z}'_{j+1/2,l}\mathbf{V}_j & \text{if } u_x + \lambda_{j+1/2,l} > 0, \\ \mathbf{z}'_{j+1/2,l}\mathbf{V}_{j+1} & \text{if } u_x + \lambda_{j+1/2,l} < 0, \end{cases} \tag{5.12}$$

for $l = 1, ..., 11$. We multiply (5.12) from the left by $(u_x + \lambda_{j+1/2,l})\mathbf{s}_{j+1/2,l}$ and add. This gives

$$(u_x\mathbf{I} + \mathbf{A})\tilde{\mathbf{V}} = (u_x\mathbf{I} + \mathbf{A})\tfrac{1}{2}(\mathbf{V}_j + \mathbf{V}_{j+1}) - \tfrac{1}{2} \sum_l |u_x + \lambda_{j+1/2,l}| \mathbf{s}_{j+1/2,l}\mathbf{z}'_{j+1/2,l}(\mathbf{V}_{j+1} - \mathbf{V}_j). \tag{5.13}$$

The left-hand side of (5.13) should be taken as the flux

on the interface for the linear equations (5.10), using the upstream differencing method. We carry this over to the nonlinear equations (5.7) by replacing the first term in (5.13) as far as possible by the corresponding nonlinear fluxes. This can be done only for the part $\partial \mathbf{F}^x/\partial \mathbf{V}$ of $\mathbf{u}_x\mathbf{I} + \mathbf{A}$. The nonconservative part $\mathbf{C}_x$ must be retained and occurs explicitly in (5.8). The first term in (5.13) alone would result in an unstable central difference scheme. The last term transforms it to a stable upwind scheme. This term is called the upstream correction.

This approach can be used also when complex eigenvalues occur. One has to replace the eigenvalues by the real parts.

This leads finally to the formula for the fluxes on the interfaces:

$$\begin{aligned}\mathbf{F}^{x,n}_{j+1/2} = {} & \tfrac{1}{2}(\mathbf{F}^x(\mathbf{V}^n_j) + \mathbf{F}^x(\mathbf{V}^n_{j+1})) \\ & - \tfrac{1}{2}|u_{x,j+1/2}|(\mathbf{W}^n_{j+1} - \mathbf{W}^n_j) \\ & - \tfrac{1}{2}\mathbf{H}\sum_l (|\mathrm{Re}\ \lambda_{j+1/2,l} + u_{x,j+1/2}| \\ & - |u_{x,j,+1/2}|)\mathrm{Re}(\mathbf{s}_{j+1/2,l}\mathbf{z}'_{j+1/2,l})(\mathbf{V}^n_{j+1} - \mathbf{V}^n_j) \\ & + \tfrac{1}{2}\mathbf{H}\sum_l \mathrm{Im}\ \lambda_{j+1/2,l}\mathrm{Im}(\mathbf{s}_{j+1/2,l}\mathbf{z}'_{j+1/2,l})(\mathbf{V}^n_{j+1} + \mathbf{V}^n_j).\end{aligned} \tag{5.14}$$

The first term in (5.14) accounts for the conservative part of the flux. The second term makes the upstream correction for all waves which have $\lambda = 0$, i.e., mainly for the advection. The third part incorporates the upstream correction for all waves with speed different from the flow speed. The last term finally removes the contribution of the term $\mathbf{A}_u\partial\mathbf{V}/\partial x$ (see (4.9)) from the spatial difference term. We call this term the instability correction. This term is artificial and optional. When this term is included the difference method is suitable to calculate the stable part of the solution as discussed in Section 4. Note that the sums in (5.14) can be confined to those l for which $\lambda_{j+1/2,l}$ is different from zero. Therefore, one needs the eigenvectors only for nonzero eigenvalues.

We have retained in (5.10) the spatial derivative of $\mathbf{V}$ instead of $\mathbf{W}$. This has the advantage that we can use for the calculation of the upstream correction the differences in $\mathbf{V}$ and not in $\mathbf{W}$. Therefore, the left eigenvectors of the matrix $\mathbf{A}$ can be used without modifications. Only the right eigenvectors of $\mathbf{A}$ have to be multiplied by the matrix $\mathbf{H}$.

For the linear equations (5.9) one would get the same result as in (5.13) by considering the Riemann problem with $\mathbf{V}_j$ and $\mathbf{V}_{j+1}$ as left and right states and taking on the interface the constant value $\tilde{\mathbf{V}}$ which develops as a result of the resolution of the discontinuity for $t > 0$ at $x_{j+1/2}$. Therefore, one can say that the method using (5.14) is based on an approximate Riemann solver [21, 18]. For conservation laws one can incorporate the upstream correction also by considering the nonlinear Riemann problem. The resulting method, first introduced by Godunov [9], has very good performance at shocks. It has no counterpart for nonconservative equations.

Formula (5.8) can easily be generalized for the system of Eq. (5.1) on a three-dimensional rectangular nonequidistant grid.

Let $x_{j+1/2}$, $y_{k+1/2}$, $z_{l+1/2}$, $j = 0, 1, ..., n_x$, $k = 0, 1, ..., n_y$, $l = 0, 1, ..., n_z$ be the coordinates of planes which subdivide a certain volume into $n_x \times n_y \times n_z$ cells T_{jkl}. For each cell there are at time $t_n = n\Delta t$ values of the variables $\mathbf{V}^n_{jkl}$. The values at time t_{n+1} are calculated as in (5.8),

$$\begin{aligned}\mathbf{W}^{n+1}_{jkl} = {} & \mathbf{W}^n_{jkl} + \Delta t\dot{\mathbf{W}}_{jkl} \\ & - \frac{\Delta t}{\Delta x_j}\left(\mathbf{F}^x_{j+1/2kl} - \mathbf{F}^x_{j-1/2kl} + \mathbf{C}_x(\mathbf{V}^n_{jkl})\frac{\mathbf{V}_{j+1kl} - \mathbf{V}_{j-1kl}}{2}\right) \\ & - \frac{\Delta t}{\Delta y_k}\left(\mathbf{F}^y_{jk+1/2l} - \mathbf{F}^y_{jk-1/2l} + \mathbf{C}_y(\mathbf{V}^n_{jkl})\frac{\mathbf{V}_{jk+1l} - \mathbf{V}_{jk-1l}}{2}\right) \\ & - \frac{\Delta t}{\Delta z_l}\left(\mathbf{F}^z_{jkl+1/2} - \mathbf{F}^z_{jkl-1/2} + \mathbf{C}_z(\mathbf{V}^n_{jkl})\frac{\mathbf{V}_{jkl+1} - \mathbf{V}_{jkl-1}}{2}\right),\end{aligned} \tag{5.15}$$

with $\Delta x_j = x_{j+1/2} - x_{j-1/2}$ and similar for the other coordinates. The fluxes on the interfaces are calculated in a similar way as in the one-dimensional case. Formula (5.14) can be generalized. For instance, the flux $\mathbf{F}^x_{j+(1/2)kl}$ on an interface is the mean of the fluxes in the adjacent cells calculated from $\mathbf{V}_{jkl}$ and $\mathbf{V}_{j+1kl}$ with an upstream and instability correction which is determined with the eigensystem of the matrix $\mathbf{A}_x$ calculated with the mean value of $\mathbf{V}_{jkl}$ and $\mathbf{V}_{j+1kl}$ and the normal $\mathbf{k} = (1, 0, 0)'$.

By (5.8) the state $\mathbf{V}^{n+1}$ at time t_{n+1} is calculated from the state $\mathbf{V}^n$ by the application of an operator $\mathbf{L}_x$. This operator can be studied for Eq. (5.7) in the case of an initial state $\mathbf{V}$ which is a constant steady state $\mathbf{V}_0$ plus a small disturbance $\mathbf{V}_1$. We consider Eq. (5.7) without source terms and with periodic boundary conditions.

We use the abbreviation $\nu = \Delta t/\Delta x$. With the spectral representation of the Jacobi matrix of the undisturbed state $\mathbf{V}_0$,

$$\mathbf{A} = \mathbf{A}(\mathbf{V}_0) = \sum_l \lambda_l \mathbf{s}_l \mathbf{z}'_l, \tag{5.16}$$

and Fourier analysis the initial state at grid point x_j can be written as

$$\mathbf{V}^0_j = \sum_{k,l} a_{kl}\mathbf{s}_l \exp\left(i\frac{jk2\pi}{N}\right). \tag{5.17}$$

The state after one time step is then

$$\mathbf{V}_j^1 = \sum_{k,l} f_{kl} a_{kl} \mathbf{s}_l \exp\left(i \frac{jk2\pi}{N}\right). \tag{5.18}$$

The amplification factors f_{kl} depend on the method applied. If only the uncorrected fluxes are applied, i.e., the first term in (5.14), then

$$f_{kl} = 1 + \nu \mathrm{Im}\ \lambda_l \sin\frac{k2\pi}{N} - i\nu(\mathrm{Re}\ \lambda_l + u_x)\sin\frac{k2\pi}{N}. \tag{5.19}$$

For each fixed l these points are on a straight line segment which is symmetric with respect to the point 1.

With upstream correction the amplification factors are

$$f_{kl} = 1 + \nu \mathrm{Im}\ \lambda_l \sin\frac{k2\pi}{N} - i\nu(\mathrm{Re}\ \lambda_l + u_x)\sin\frac{k2\pi}{N} - \nu|\mathrm{Re}\ \lambda_l + u_x|\left(1 - \cos\frac{k2\pi}{N}\right). \tag{5.20}$$

If λ_l is real this is a circle with radius $\nu|\mathrm{Re}\ \lambda_l + u_x|$. This circle is symmetric with respect to the real axis and passes through the point 1. It is inside the unit circle if and only if

$$\nu|\mathrm{Re}\ \lambda_l + u_x| < 1. \tag{5.21}$$

This is the well-known Courant–Friedrichs–Lewy condition for stability.

If λ_l is complex then (5.20) describes an ellipse which passes through 1 but is not tangent to the unit circle. Therefore, the magnitude of f_{kl} can exceed 1.

If in addition the instability correction is applied, the amplification factors

$$f_{kl} = 1 - i\nu(\mathrm{Re}\ \lambda_l + u_x)\sin\frac{k2\pi}{N} - \nu|\mathrm{Re}\ \lambda_l + u_x|\left(1 - \cos\frac{k2\pi}{N}\right) \tag{5.22}$$

lie on the same circle as in the case of real λ_l described before.

6. NUMERICAL EXPERIMENTS AND RESULTS

(a) *One-dimensional calculations*

First we calculate a one-dimensional flow where all variables depend only on the x-coordinate. We treat several model situations where the different types of instabilities occur. As initial conditions we use a constant state with a small random disturbance. The calculations are done on a grid with 30 points and gridsize $\Delta x = 1$. Periodic boundary conditions are applied so that the waves can travel around the grid unimpeded. The parameters of the constant state for the four models are listed in Table I. We use CGS units and put $\gamma = \frac{5}{3}$ and $\mu = 4\pi$.

TABLE I

Parameters for One-Dimensional Test Calculations

Model	1	2	3	4
n	1	1	1	1
ρ	1	1	1	1
p_e	1	1	1	1
$p_\perp$	1	1	1	10
$p_\parallel$	1	5	5	.5
u_x	1	1	1	1
u_y	.2	.2	.2	.2
u_z	0	0	0	0
B_x	3.5	3.5	5	3.5
B_y	3.5	3.5	1	3.5
B_z	0	0	0	0
Δt	.3	.25	.15	.15
λ_1^2	4.58	8.58	16.00	23.5
λ_2^2	1.54	1.51	−1.64	−.09
λ_3^2	.97	−1.02	−1.85	.44

The flow in model 1 is stable since the pressure is isotropic. In model 2 the parallel pressure dominates so much that condition (4.1) is satisfied and the firehose instability occurs.

If the angle θ between field and wave vector is less than 32° then also λ_2^2 becomes negative. This occurs in the configuration of model 3. In model 4 the perpendicular pressure is much larger than the parallel pressure so that the condition (4.3) is satisfied. The mirror instability occurs for $\theta > 37°$. This is the case for the given field orientation.

The amplification factors for these models are shown in Fig. 1. For the stable model 1 all waves are damped. In the last three models amplification factors of magnitude larger than 1 occur if only upstream correction is applied. This implies that there are growing modes. If instability correction is implemented the amplification factors for the unstable modes are changed and coincide with those of convection (the dashed lines in Fig. 1). Then all amplification factors have magnitude less than or equal to 1.

An indicator for convergence is the L^1 norm d_n of the change $\mathbf{D}^n := \mathbf{V}^n - \mathbf{V}^{n-1}$ in the nth time step. For model 1 d_n decreases monotonically and the sequence $\mathbf{V}^n$ converges to the underlying constant state. For the other models in calculations without instability corrections the norm d_n of the change first increases then also decreases monotonically and the $\mathbf{V}^n$ converges to a constant state. But this final state is different from the initial constant state. The difference is only in the pressures which are changed to $p_\perp = 1.25$, $p_\parallel = 3.28$ in model 2, to $p_\perp = 1.25$, $p_\parallel = 3.28$ in model 3, and to $p_e = 1.13$, $p_\perp = 7.82$, $p_\parallel = 3.01$ in model 4. Hence the instability effects an isotropization which

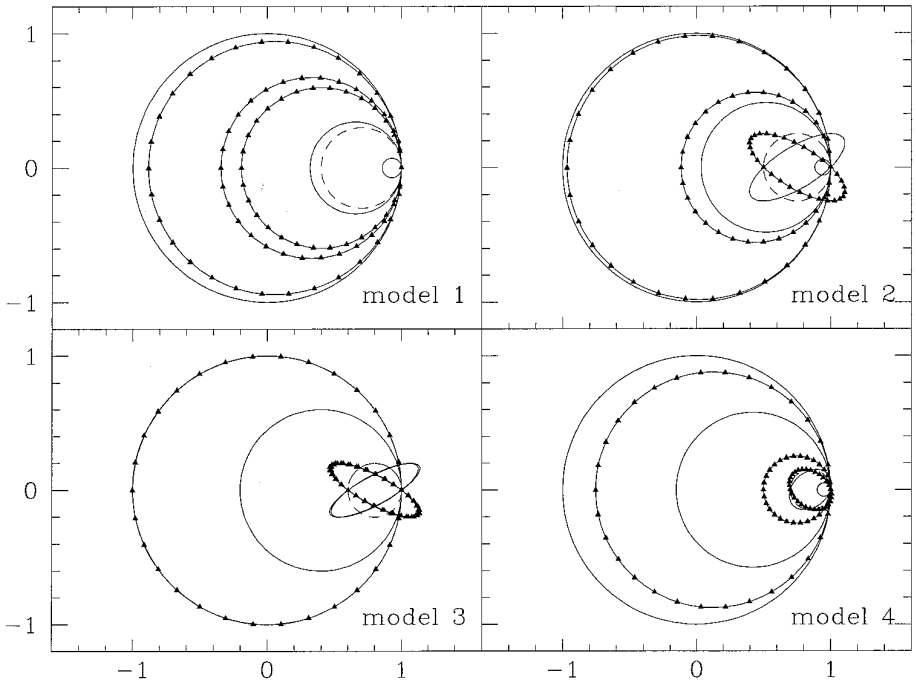

FIG. 1. The amplification factors for the different waves and the model parameters listed in Table I for the method with upstream correction only. Solid line for waves with $\lambda \neq 0$ and dashed for convection ($\lambda = 0$). The triangles mark for waves with Re $\lambda > 0$ or Im $\lambda > 0$ the points which correspond to waves on the grid.

stabilizes the flow. When this change in the state occurs the time evolution switches from divergence to convergence. Figure 2 shows the L^1 norm of $p_\perp^n - p_\perp^{n-1}$ and the average value of the pressure components $p_\parallel$ and $p_\perp$ in each time step.

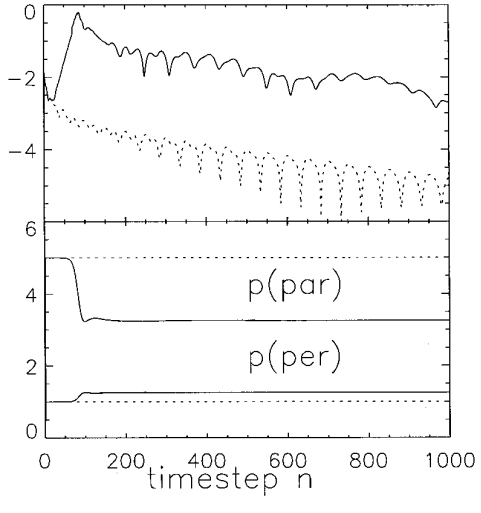

FIG. 2. Top panel: The logarithm of the L^1 norm of $p_\perp^n - p_\perp^{n-1}$ in time step n. Bottom panel: The average values of $p_\perp$ and $p_\parallel$. The results are from calculations for model 3 with instability correction (dotted line) and without (solid line).

With instability correction, d_n decreases on the average with small oscillations. The solution converges to a constant state which coincides with the undisturbed initial state.

It is interesting to follow the transition to a new state in more detail. We calculate in model 3 a sine wave corresponding to the eigenvalue λ_1 on a grid with 100 points for 1500 timesteps. Although this wave is stable it generates via the nonlinear terms waves corresponding to the eigenvalue λ_2. These waves are unstable. If no instability correction is made these waves grow linearly. After the first 200 timesteps they grow much faster since they are more efficiently amplified by the original wave, whose amplitude decreases. For a short time a sort of white noise occurs, from which a new configuration emerges with a new background state. The pressures have changed to $p_\perp = 1.31, p_\parallel = 3.04$. This state is stable. In Fig. 3 we show the evolution of the perpendicular pressure with time on the grid. The most conspicuous feature is finally a sawtooth discontinuity which moves with the fluid.

In Fig. 4 we show the magnitude of the first Fourier coefficients of the perpendicular pressure for the 1500 timesteps. The coefficient with index 0 measures the average value. It changes around timestep 300 from 1 to 1.31. The coefficient with index 1 measures the original sine wave. The waves with shorter wavelength are excited and grow so that they attain the same amplitude as the original

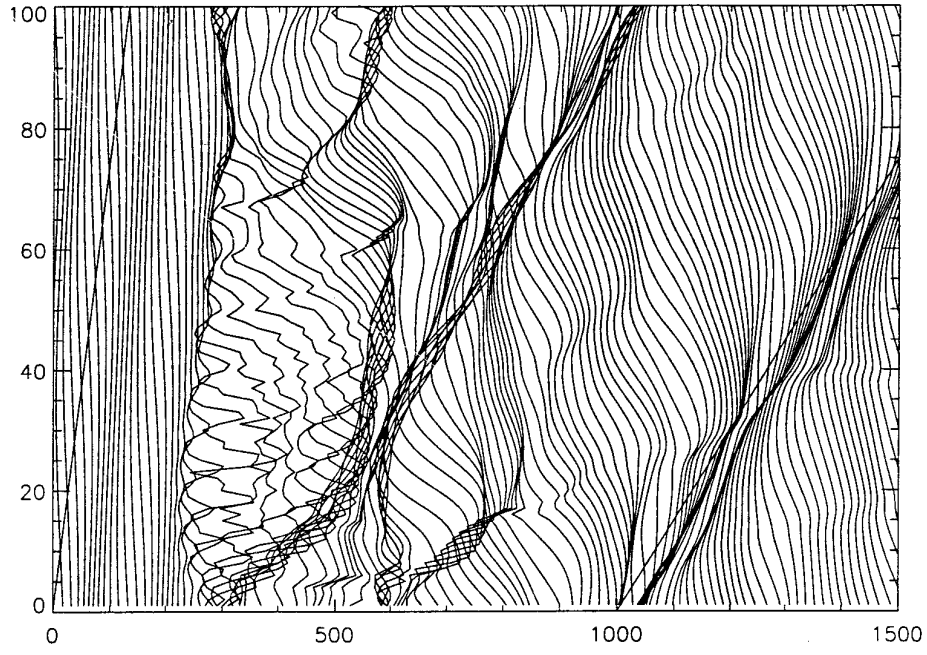

FIG. 3. The values of the perpendicular pressure $p_\perp(t, x)$. The ordinate denotes x. The curves are shifted. Each line shows $p_\perp(t_n, x)$ (arbitrary units) at a certain time step t_n with n labelled by the abscissa. The straight lines starting at $n = 0$ and $n = 1000$ mark the propagation of the original wave and the final convected sawtooth.

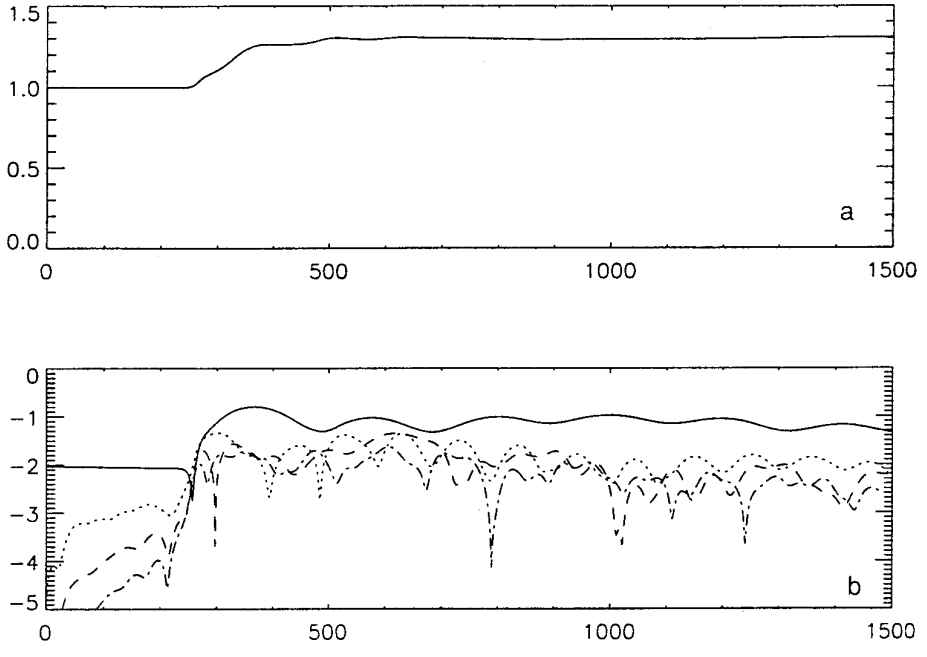

FIG. 4. Magnitude of the Fourier coefficients of $p_\perp$ as a function of the time step (abscissa): (a) The coefficient with index 0 measures the average value (linear scale). (b) The coefficients with index 1 (solid), 2 (dotted), 3 (dashed), and 4 (dash-dotted) in logarithmic scale.

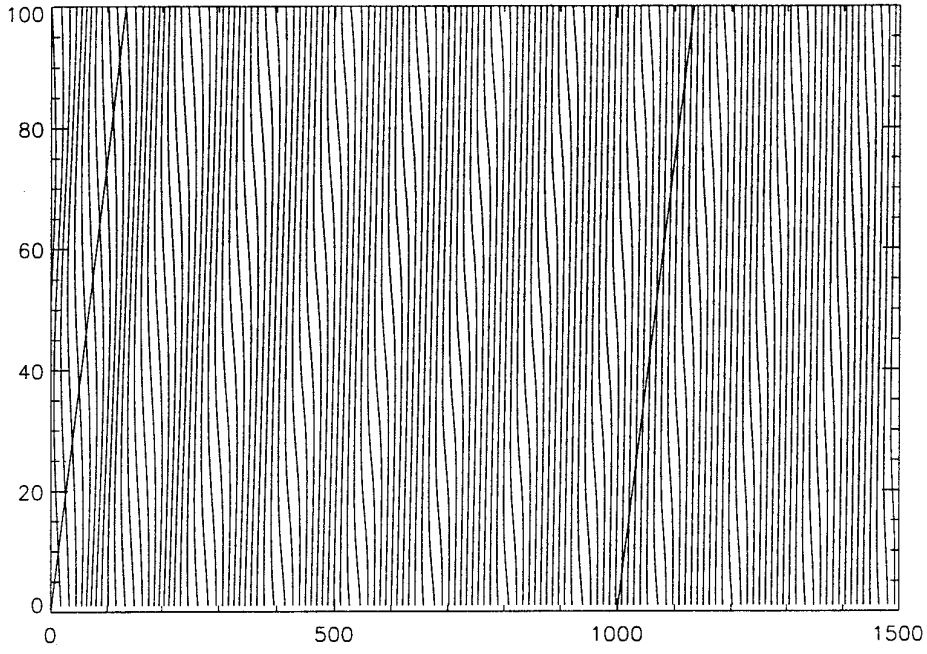

FIG. 5. The same as Fig. 3 but for a calculation with instability correction.

wave. In this way a sort of white noise is generated. After the transition to the new state the waves survive. But they are now more coherent and combine to a sawtooth function.

If the instability correction is implemented the original wave remains undisturbed during the whole calculation (see Fig. 5). It is only damped due to the numerical diffusion. Shorter waves are excited by the nonlinear terms. But their amplitude remains well below that of the original wave (see Fig. 6).

(b) *Three-Dimensional Calculations*

In three dimensions the situation is more complicated for several reasons. The spatial differential operator is represented as the sum of three one-dimensional difference operators. Even if each of these damps all waves according to the one-dimensional analysis the complete operator may well amplify waves. The three operators do not commute. Therefore, the damping does not hold with respect to a common basis system. The instabilities depend in a crucial way on the angle to the magnetic field. Therefore, the instability correction in general does not help.

(c) *The Comet*

For the cometary model one has to provide the source terms on the right-hand side of (2.1) to (2.6). The nucleus of the comet releases G particles per second which stream radially away with a velocity w. The mean mass of a cometary particle is m_C. It is ionized with a rate σ. The density n_n of neutral particles depends only on the distance r to the nucleus

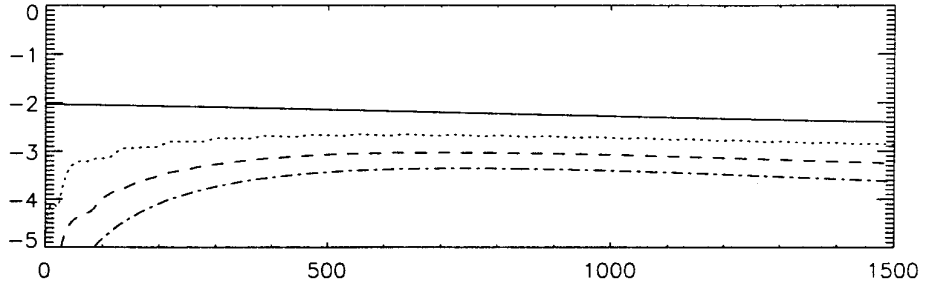

FIG. 6. The same as Fig. 4b but for a calculation with instability correction.

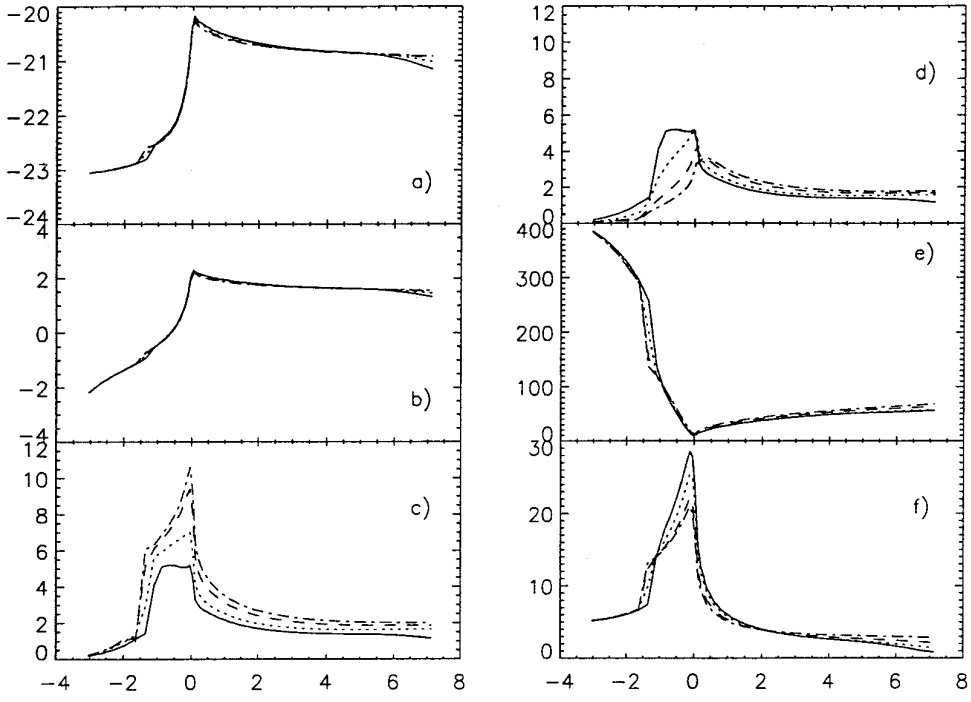

FIG. 7. The values along the sun–comet axis for different values of $t_{\rm iso} = 1$ (solid line), 300 (dotted), 1000 (dashed), and 1800 s (dashed-dotted). The abscissa shows the distance z (100,000 km): (a) mass-density (logarithm) (g/cm^3); (b) ion density (logarithm) (cm^{-3}); (c) perpendicular pressure (10^{-9} dyn/cm^2); (d) parallel pressure (10^{-9} dyn/cm^2), (e) velocity (km/s); (f) magnetic field (10^{-5} Gs).

$$n_n = \frac{G}{4\pi w r^2} \exp\left(-\frac{r\sigma}{w}\right). \tag{6.1}$$

The source terms are proportional to the neutral density

$$\dot{n} = \sigma n_n, \quad \dot{p} = m_C \dot{n}, \quad \dot{\mathbf{q}} = \dot{p}\mathbf{w},$$
$$\dot{p}_\perp = \tfrac{1}{2}\dot{p}(\mathbf{u}_\perp - \mathbf{w}_\perp)^2, \quad \dot{p}_\parallel = \dot{p}(\mathbf{u}_\parallel - \mathbf{w}_\parallel)^2. \tag{6.2}$$

The kinetic energy of the new ions in the plasma rest frame contributes to the thermal energy of the plasma. The part perpendicular to the field is added to the perpendicular pressure, the parallel part to the parallel pressure. The kinetic energy must be multiplied by the factor $\gamma - 1$ which is 1 for $p_\perp$ and 2 for $p_\parallel$. This gives the source terms in (6.2). For this mainly illustrative calculation we put $\dot{p}_e = 0$.

We calculate with the following parameters for the comet $G = 10^{29} s^{-1}$, $w = 1$ km/s, $m_C = 20$ atomic mass units (amu), $\sigma = 10^{-6} s^{-1}$. We start the calculation from a constant state equal to the solar wind condition $n = 5$ cm^{-3}, $\rho = 5$ amu/cm^3, $\mathbf{u} = (0, 0, 400)$ km/s, $\mathbf{B} = (5\ 10^{-5}, 0, 0)$ Gs, $p_e = 1.73\ 10^{-10}$ dyn/cm^2, $p_\perp = p_\parallel = 6.9\ 10^{-11}$ dyn/cm^2.

It is well known from measurements at comet Halley that various processes are effective which scatter the pitch angle and so isotropize the plasma [16]. We take this into account by an exponential decay of the anisotropy with a time scale $t_{\rm iso}$. In each time step we replace $p_\perp$, $p_\parallel$ by

$$(1-\beta)p_\perp + \beta p_{\rm iso}, \quad (1-\beta)p_\parallel + \beta p_{\rm iso} \tag{6.3}$$

with $\beta = \min(1, \Delta t/t_{\rm iso})$ and the isotropic pressure $p_{\rm iso} = \frac{2}{3}p_\perp + \frac{1}{3}p_\parallel$.

We calculate on a nonequidistant grid with $14 \times 14 \times 46$ grid points which cover the range $0 \le x, y \le 300{,}000$ km, $-300{,}000 \le z \le 700{,}000$ km. The best resolution of 8000 km is near the nucleus. At $x = 0$ and $y = 0$ we apply symmetry boundary conditions, at $z = -300{,}000$ km the boundary values are solar wind data. At all other boundaries gradient zero is assumed.

We calculate for different values of $t_{\rm iso} = 1$, 300, 1000, and 1800 s. The flow is everywhere stable for the small values of $t_{\rm iso}$. For $t_{\rm iso} = 1800$ mirror instability occurs in a region close to the axis at a distance of about 100,000 km in front of the nucleus. Nevertheless this model also approaches a steady state. We discuss in the following the state after 6 h real time which is already close to stationary.

Figure 7 shows the values along the sun–comet axis. There is a detached bow shock in front of the nucleus at a distance of about 150,000 km. For increasing values of $t_{\rm iso}$ the shock moves farther out. It has been shown by Biermann *et al.* [1] that the shock distance is approximately

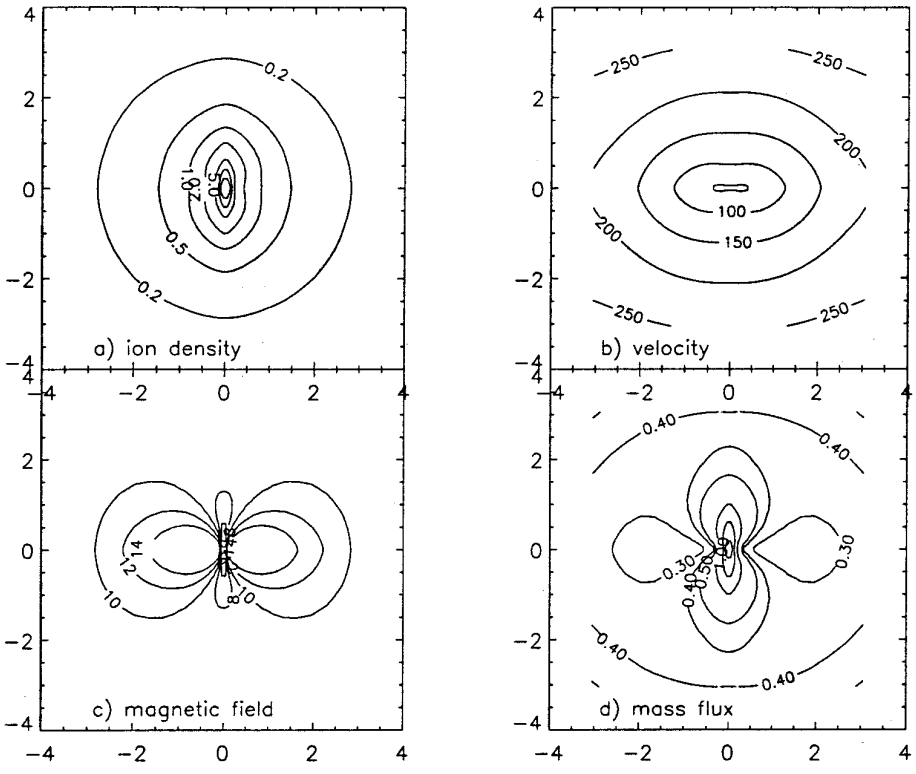

FIG. 8. Cut perpendicular to the tail at a distance 393,000 km behind the nucleus for $t_{\rm iso} = 1$ s. The length scale is in 100,000 km. The orientation of the interplanetary magnetic field is horizontal: (a) ion density (cm^{-3}); (b) velocity (km/s); (c) magnetic field (10^{-5} Gs); (d) mass flux ρu_z (10^{-15} g/s cm^2).

$$R_s \approx (\gamma^2 - 1)\frac{\sigma m_C G}{4\pi w \rho_\odot u_\odot}, \tag{6.4}$$

where $\rho_\odot u_\odot$ is the mass flux of the solar wind. In this formula the γ depends on the degrees of freedom to which the heat generated by the ion pickup is distributed. For isotropic pressure there are three degrees of freedom and $\gamma = \frac{5}{3}$. But for anisotropic pressure only the perpendicular pressure is heated. This gives only two degrees of freedom and $\gamma = 2$.

Equations (2.1) to (2.7) are not in conservative form. We have preferred the pressure equation (2.4) over the energy equation (2.11) since we intend to generalize the approach to a multi-ion plasma, where it is even harder to get energy equations in conservative form. Nevertheless, we get a well-developed bow shock. But a closer inspection shows that, compared with previous MHD calculations or with the estimate (6.4), the shock is a little too close to the nucleus.

The magnetic field is piled up in the stagnation region in front of the nucleus until it becomes strong enough to divert the flow in such a way that the field is transported around the nucleus. The field is draped around the nucleus and the field caught in the stagnation region expands in the tail into two flux ropes of opposite polarity.

The perpendicular pressure in the stagnation region is larger by a factor of 2 in the anisotropic models. Since an anisotropic pressure helps to expand the compressed field in the direction perpendicular to the field, there is less field compression necessary to organize the transport of the field. Therefore, the magnetic field in the pileup region and in the flux tubes in the tail becomes smaller with increasing $t_{\rm iso}$. The increase in $p_\perp$ compensates nearly the reduction in magnetic pressure.

Mass density and number density of the ions in the tail depend only a little on the degree of isotropization.

Figures 8 and 9 show the state in the far tail at a distance of 393,000 km behind the nucleus for the isotropic ($t_{\rm iso} = 1$) and for an anisotropic case ($t_{\rm iso} = 1800$). Most conspicuous is the reduction of the magnetic field in the anisotropic models. Already for isotropic plasma the main mass flow in the tail is in a plane perpendicular to the field. The Lorentz forces are most efficient in this direction. Therefore, velocity and density are highest in the perpendicular plane. The tail is flattened in this direction.

Pressure anisotropy diverts the mass flux even more from the plane parallel to the field into the regions outside.

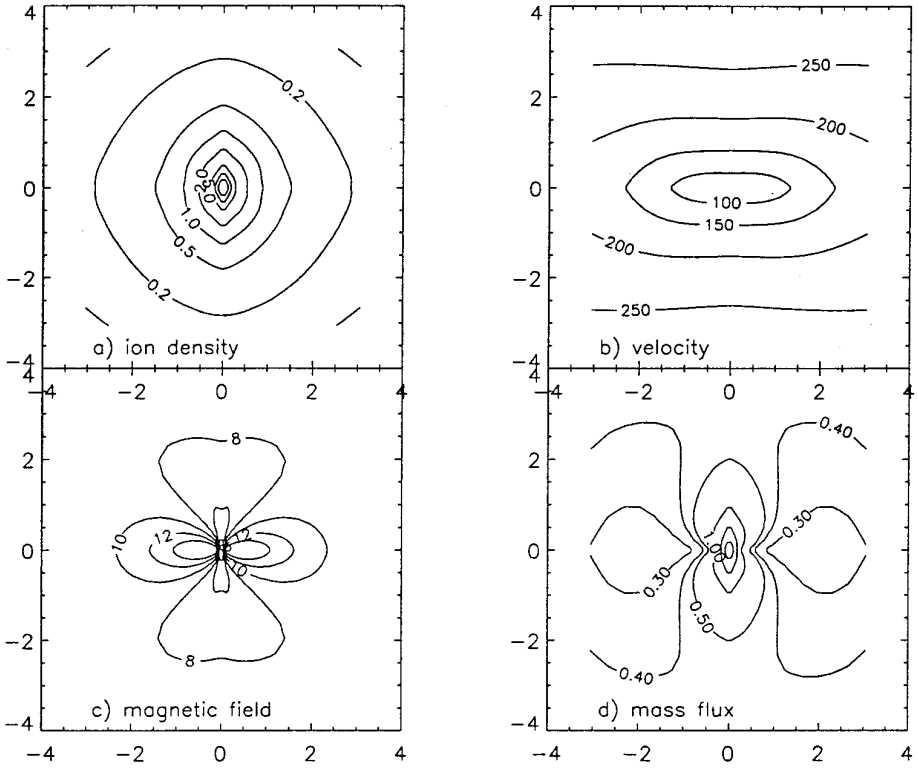

FIG. 9. The same as Fig. 8 but for $t_{iso} = 1800$ s.

The density is changed only a little. The changed mass flux is mainly due to a change in velocity. In fact, the speed is reduced in the parallel plane, but accelerated in the region far outside this plane.

Due to the reduced magnetic field the magnetic pressure on the tail is relaxed. Therefore, the tail becomes slightly less flattened.

7. CONCLUSION

We have developed an upstream differencing method for the double-adiabatic equations. The numerical scheme uses an approximate Riemann solver which is based on an explicit representation of the complete eigensystem of the Jacobian matrix of the flux vector.

The method has to be adapted in such a way that it can also cope with complex eigenvalues and eigenvectors which occur if the flow is unstable with respect to the firehose or mirror instability. A method is proposed to turn off the instabilities. This ''instability correction'' works well in one-dimensional, but not in three-dimensional, test calculations. It turns out that instabilities in general grow but finally isotropize the pressure and so stabilize the flow.

Pressure anisotropies play an important role in the plasma flow in a comet since the cometary ions at first only contribute to the perpendicular pressure which is isotropized only gradually by various processes. Numerical simulations for the interaction of the solar wind with a comet show that pressure anisotropy shifts the bow shock, reduces the magnetic field in the stagnation region and in the tail, and accelerates the flow in the plane perpendicular to the interplanetary field.

REFERENCES

1. L. Biermann, B. Brosowski, and H. U. Schmidt, The interaction of the solar wind with a comet, *Solar Phys.* **1,** 254 (1967).
2. J. U. Brackbill and D. C. Barnes, The effect of nonzero $\nabla \cdot B$ on the numerical solution of the magnetohydrodynamic equations, *J. Comput. Phys.* **35,** 426 (1980).
3. M. Brio and C. C. Wu, An upwind differencing scheme for the equations of ideal magnetohydrodynamics, *J. Comput. Phys.* **75,** 400 (1988).
4. G. F. Chew, M. L. Goldberger, and F. E. Low, The Boltzmann equation and the one-fluid hydromagnetic equations in the absence of particle collisions, *Proc. Roy. Soc. A* **236,** 112 (1956).
5. R. Courant, E. Isaacson, and M. Rees, On the solution of nonlinear hyperbolic differential equations by finite differences, *Commun. Pure Appl. Math.* **5,** 243 (1952).
6. W. Dai and P. R. Woodward, An approximate Riemann solver for ideal magnetohydrodynamics, *J. Comput. Phys.* **111,** 354 (1994).
7. W. Dai and P. R. Woodward, Extension of the piecewise parabolic method to multidimensional ideal magnetohydrodynamics, *J. Comput. Phys.* **115,** 485 (1994).

8. P. R. Garabedian, *Partial Differential Equations* (Wiley, New York, 1964).
9. S. K. Godunov, Finite difference method for numerical computation of discontinuous solutions of the equations of fluid dynamics, *Math. Sb.* **47,** 271 (1959).
10. T. I. Gombosi, K. G. Powell, and D. L. De Zeeuw, Axisymmetric modelling of cometary mass loading on an adaptively refined grid: MHD results, *J. Geophys. Res.* **99,** 21,525 (1994).
11. M. Hesse and J. Birn, MHD modeling of magnetotail instability for anisotropic pressure. *J. Geophys. Res.* **97,** 10643 (1992).
12. A. Jeffrey and T. Taniuti, *Non-linear Wave Propagation* (Academic Press, New York, 1964).
13. R. J. LeVeque, *Numerical Methods for Conservation Laws* (Birkhäuser, Basel, 1992).
14. R. Lüst, Über die Ausbreitung von Wellen in einem Plasma, *Fortsch. Phys.* **9,** 503 (1959).
15. C. D. Munz, On Godunov-type schemes for Lagrangian gas dynamics, *SIAM J. Numer. Anal.* **31,** 17 (1994).
16. M. Neugebauer, A. J. Lazarus, K. Altwegg, H. Balsiger, B. E. Goldstein, R. Goldstein, F. M. Neubauer, H. Rosenbauer, R. Schwenn, E. G. Shelley, and E. Ungstrup, The pick-up of cometary protons by the solar wind, *Astron. Astrophys.* **187,** 21 (1987).
17. N. Panofsky and M. Phillips, *Classical Electricity and Magnetism* (Addison–Wesley, Reading, MA, 1962).
18. P. L. Roe, Approximate Riemann solvers, parameter vectors, and difference schemes, *J. Comput. Phys.* **43,** 357 (1981).
19. D. Ryu and T. W. Jones, Numerical magnetohydrodynamics in astrophysics: Algorithms and tests for one-dimensional flow, *Astrophys. J.* **442,** 228 (1995).
20. D. Ryu, T. W. Jones, and A. Frank, Numerical magnetohydrodynamics in astrophysics: Algorithm and tests for multidimensional flow, *Astrophys. J.* **452,** 785 (1995).
21. H. U. Schmidt and R. Wegmann, MHD calculations for cometary plasmas, *Comput. Phys. Commun.* **19,** 309 (1980).
22. H. U. Schmidt and R. Wegmann, Plasma flow and magnetic fields in comets, *in Comets,* edited by L. L. Wilkening (Univ. of Arizona Press, Tucson, AZ, 1982), p. 538.
23. T. Tanaka, Configurations of the solar wind flow and magnetic field around the planets with no magnetic field: Calculation by a new MHD simulation scheme, *J. Geophys. Res.* **98,** 17,251 (1993).
24. A. Zachary and P. Colella, A higher-order Godunov method for the equations of ideal magnetohydrodynamics, *J. Comput. Phys.,* **99,** 341, 1992.
25. A. Zachary, A. Malagoli, and P. Colella, A higher-order Godunov method for multidimensional ideal magnetohydrodynamics, *SIAM J. Sci. Comput.* **15,** 263 (1994).